

ON THE MODAL ANALYSIS OF FAST RESPONSE AERODYNAMIC PRESSURE PROBE DATA

L. Simonassi, M. Zenz, S. Zerobin,
F. Heitmeir, A. Marn

Institute of Thermal Turbomachinery and Machine Dynamics
Graz University of Technology, Austria

T. Selic

Elin Motoren GmbH
Weiz, Austria

Keywords: modal analysis, fast response pressure probe, low pressure turbine

ABSTRACT

This paper presents the analysis procedure adopted to study the unsteady aerodynamic measurement data obtained from a Fast Response Aerodynamic Pressure Probe (FRAPP) downstream of a low pressure turbine (LPT) rotor in a 1.5-stage turbine test rig. The method, which is based on the acoustic theory of Tyler and Sofrin, focuses on the investigation of the main structures constituting the unsteady flow field.

In the last section of this paper, an example of applying the mentioned technique onto experimental data obtained in a subsonic turbine test facility is shown. The interactions between the stator and rotor wakes, secondary flows and the turbine exit guide vanes (TEGVs) potential effect are identified, and their importance in the assessment of the aerodynamic and aeroelastic performance of modern low pressure turbines is analysed.

NOMENCLATURE

Abbreviations

BPF	Blade Passing Frequency
BPP	Blade Passing Period
FF	Fourier – Filtering
FRAPP	Fast Response Aerodynamic Pressure Probe
LPT	Low Pressure Turbine
STTF-	Subsonic Test Turbine Facility for
AAAI	Aerodynamic, Acoustic, and Aeroelastic Investigations
TEC	Turbine Exit Casing
TEGV	Turbine Exit Guide Vane

Symbols

A	Complex amplitude
B	Number of Blades
c	Speed of sound
f	Frequency, modal shape factor
h	Harmonic index
k	Axial wave number
m	Azimuthal mode order
n	Radial mode order, Rotor speed
N	Circumferential measurement point

p	Pressure
r	Radius
t	Time
T	Temperature
v	Velocity
V	Number of vanes
x	Space coordinate

Greek Symbols

φ	Circumferential coordinate
θ	Inclination angle
τ	Period
ω	Angular frequency
Ω	Angular speed
α	Cut-on factor
	$= \sqrt{1 - (1 - M_x^2) \frac{\sigma_{mn}^2}{(kR)^2}}$
σ	Eigenvalues of the Bessel function

Subscript

ax	Axial
m	Azimuthal mode order
n	Radial mode order
s	Scattered
t	Total
φ	Circumferential coordinate
Vane	Vane pitch

Superscript

\pm	Propagation in (+) and against (-) flow direction
\sim	Area average
$\langle \rangle$	Purely periodic component
'	Stochastic fluctuation component
$-$	Time average component

INTRODUCTION

The unsteady interaction between stator vanes and rotor blades influence significantly not only the aerodynamic performances of turbomachinery, but also have a strong effect on the noise emission and on the blade vibration of the rotor.

Investigations based on the modal decomposition proposed by Tyler and Sofrin [1] showed that superimposed circumferential and radial pressure patterns were identified as the origin

of acoustic noise emissions. Lengani et al. [2] applied the modal theory to unsteady aerodynamic measurement data obtained in a turbine test rig and proved that the mode detection technique can be successfully applied to get a deeper insight into the unsteady flow field. Zerobin et al [3] discussed the unsteady stator-rotor interaction in a turbine test rig including a turbine center frame duct.

The present work presents the post-processing methodology of unsteady aerodynamic data applied to decompose a complex flow field downstream of a LPT rotor. Additionally, the last section demonstrates the application of this methodology onto experimental data obtained in a 1.5 stage LPT.

METHODOLOGY OF THE MODE ANALYSIS

Determination of Stochastic Pressure Fluctuations

Fourier-filtering (FF) is adopted to identify the stochastic pressure fluctuations from a FRAPP, as described by Lengani et al. [4] and Camp and Shin [5]. The post-processing is based on the triple decomposition procedure of the measured value, which is stated in Equation (1).

$$p_t(t) = \overline{p_t(t)} + \langle p_t(t) \rangle + p'_t(t) \quad (1)$$

In this case the measured value is the total pressure, which consists of the time-averaged part $\overline{p_t(t)}$, the periodic fluctuations $\langle p_t(t) \rangle$, and the stochastic fluctuations $p'_t(t)$. The latter part is mainly associated with turbulence.

To be able to determine the stochastic fluctuations, the periodic as well as the time-averaged part have to be removed. Therefore, Fast Fourier Transformations (FFT) are executed. To reach a satisfactory frequency solution, an adequate high number of samples has to be chosen. Since no trigger signal and no averaging procedure is applied to these FFT's, the spectrum shows a peak at the rotor blade passing frequency (BPF) and its higher harmonics. In order to remove the periodic part of the pressure, these amplitudes are set to zero. The time-averaged part is eliminated by setting the amplitude at the frequency 0 Hz to zero.

The resulting spectrum is then transformed back into the time domain where then only the stochastic part of the data is remaining. That means that the result represents the time-resolved stochastic fluctuations of the total pressure $p'_t(t)$. After adaptive resampling and phase averaging to one revolution of the rotor, the RMS value of the fluctuations is calculated. It is not possible to differ between the deterministic and the stochastic part when looking at a peak of the BPF. Since the value of this peak is set to zero, a small error is made at these specific frequencies.

Mode Analysis

In order to describe the sound generating mechanisms, Tyler and Sofrin [1] wrote the pressure fluctuations at any circumferential positions downstream of a compressor stage as a sum of harmonics, represented by a Fourier series. The theoretical model they proposed has been verified by numerous aeroacoustic experimental investigations. Furthermore, there are numerous publications which show that this theory is also valid for turbines (e.g. [6], [7], [8], [9]).

Equation (2) shows the solution of the wave equation in cylindrical coordinates and for a single frequency component ω . It is given by a linear superposition of modal terms.

$$v(x, r, \varphi, t) = \sum_{m=-\infty}^{\infty} \sum_{n=0}^{\infty} (A_{mn}^{\pm} e^{ik_{mn}^{\pm} x}) f_{mn} e^{im\varphi} e^{-i\omega t} \quad (2)$$

where A_{mn}^{\pm} are the complex amplitudes downstream (-) and upstream (+), respectively. m is the azimuthal mode order and n the radial one. The factors $k_{mn}^{\pm} = \frac{\tilde{k}}{1 - \text{Ma}_{\text{ax}}^2} [-\text{Ma}_{\text{ax}}^2 \pm \alpha_{mn}]$ are the axial wave number upstream (-) and downstream (+), respectively. $\tilde{k} = \frac{\omega}{c} - m \frac{\Omega}{c}$ is a modification of the wave number definition (Morfey [10]).

The azimuthal mode amplitude for a fixed frequency can be calculated as

$$A_m(x, r)_f = \frac{1}{N_{\varphi}} \sum_{k=1}^{N_{\varphi}} p(x, r, \varphi_k)_f \cdot e^{-im\varphi_k} \quad (3)$$

N_{φ} stands for the entire number of circumferential measurement points and φ_k describes any circumferential position.

A decomposition of a variable in time and space was provided by Tyler and Sofrin. The circumferential (azimuthal) mode orders excited by the relevant airfoil interactions in turbomachinery devices can be calculated as follows:

$$\begin{aligned} m &= -h \cdot B + k \cdot V; \\ k &= -\infty, \dots, -1, 0, 1, \dots, +\infty \end{aligned} \quad (4)$$

With the vane and blade counts V and B , respectively, the harmonic index h (1 for the 1st BPF, 2 for the 2nd BPF, etc.; $BPF = B \cdot n/60$), and the integer index k . The negative sign in front of the harmonic index results in the a mathematically negative rotational direction of the rotor, which is later used in the sample shown in this work.

If there is more than one vane row in the assembly, it is possible to simply superimpose the effect of the single event. The scattering of acoustic modes m_s when interacting with a following vane row can then be written as shown in Equation (5).

Herein, V_2 is the vane count of the additional vane row.

$$\begin{aligned} m_S &= m + k \cdot V_2; \\ k &= -\infty, \dots, -1, 0, 1, \dots + \infty \end{aligned} \quad (5)$$

Associated with the azimuthal mode order m , each circumferential pressure pattern rotates at a different speed. This depends on the number of blades B and the rotational speed with the corresponding angular velocity Ω . The mode angular speed can be written as

$$\Omega_m = \frac{B}{m} \cdot \Omega \quad (6)$$

In this equation, the spinning direction of positive modes is against the rotational direction of the rotor while negative modes have the same rotational direction like the rotor.

Lengani et al. [11] proved that the modal theory model shown before is not only limited to the pressure field. It is also valid to every other aerodynamic quantity like Mach number or yaw angle. Hence, it is possible to analyse the unsteady data obtained by FRAPP measurements using the modal decomposition. According to Equation (3), the maximum mode to be calculated depends on the number of circumferential measurement positions. To be able to compute the minimum mode as well as to determine the modal structures correctly one has to ensure that the periodicity of the test setup is covered. Therefore, it is necessary to have a large enough domain of circumferential measurement points.

Time-space-diagrams are instruments to visualize as well as to qualitatively discuss the modal structures of an unsteady flow. Looking at those diagrams, the propagation of an azimuthal mode is given by its velocity v_m . In Equation (7) one can see the dependency of the velocity to the radial position r and the mode angular speed Ω_m .

$$v_m = r \cdot \Omega_m \quad (7)$$

Each mode velocity has a specific inclination in the time-space-diagrams since the velocity is defined as the rate of change of position with respect to time. For a fixed radial position, the inclination equals the mode spinning speed.

$$\frac{\Delta x}{\Delta t} = v_m \rightarrow \frac{r \cdot \Delta \varphi_k}{\Delta t} = r \cdot \Omega_m \quad (8)$$

$$\Delta \varphi_k = \Omega_m \cdot \Delta t \quad (9)$$

After combining Equation (6) and (9), the change of the circumferential position in degree can be written as follows.

$$\begin{aligned} \Delta \varphi_k &= \Omega_m \cdot \Delta t \\ &= \frac{B}{m} \cdot \Omega \cdot \Delta t \\ &= \frac{B}{m} \cdot 2\pi \frac{n}{60} \cdot \Delta t \\ &= \frac{B}{m} \cdot 2\pi \frac{n}{60} \cdot \frac{60}{n \cdot B} \cdot \frac{180}{\pi} \\ &= \frac{360}{m} \end{aligned} \quad (10)$$

Herein, one blade passing period ($BPP \triangleq \frac{t}{\tau} = 1$) for the time period Δt is considered. Equation (10) shows clearly that the inclination for one BPP only depends on the azimuthal mode order m .

When looking on the normalized time-space-diagram, the inclination and the corresponding inclination angle θ depend on a simple relation between the vane count V and the azimuthal mode order m , as can be seen in Equation (11) and (12). The normalization is done by using the normalized circumferential coordinate with respect to one vane pitch.

$$\frac{t}{\tau} = 1 \rightarrow \frac{\Delta \varphi_k}{\Delta \varphi_{vane}} = \frac{\frac{360}{m}}{\frac{360}{V}} = \frac{V}{m} \quad (11)$$

$$\frac{\Delta \varphi_k}{\Delta \varphi_{vane}} = \tan(\theta) \quad (12)$$

360 deg FRAPP Expansion

Concerning the geometrical parts of an investigated set-up as well as the limitations due to the measurements, it is difficult to acquire data over the spatial periodicity. In such a case, the measured data has to be expanded in the circumferential direction. Therefore, at a certain circumferential point the obtained data has to be shifted in time because the relative position of the rotor with respect to the stator is different in each circumferential measurement point.

As a starting point, one can consider that the stator, the rotor, and the probe are aligned as shown in Figure 1 with the position 1. After a certain number of measurement positions the probe reaches position 2, which is equal to a stator pitch. There, the rotor has a phase shift $\Delta \varphi$ with respect to the stator and the probe with the phase of $\Phi - \Delta \varphi$. Therefore, this phase shift after every following stator pitch until the total annulus of the machine has to be taken into account, to be able to recover the same combination as in the first measurement point. With every multiple of the stator pitch, the phase shift increases in the same way, e.g. after two pitches the phase is equal to $2 * (\Phi - \Delta \varphi)$ the phase shift can be written as

$2 * \Delta\varphi$ and so on until the periodicity is achieved. As a last step the shifted data can be copied in the circumferential direction to obtain the full 360 deg of the measured test set-up. An important assumption for this methodology is that the result is periodic for each stator pitch.

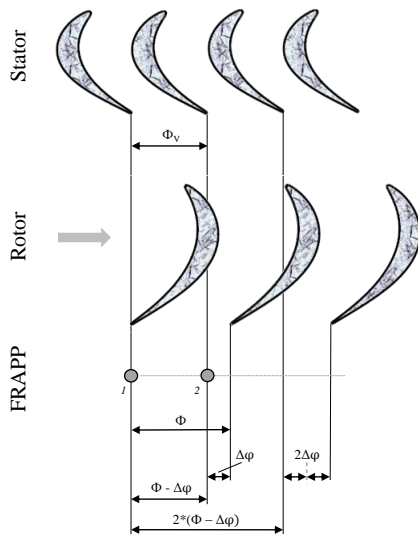


Figure 1: Scheme of the expansion methodology

EXPERIMENTAL SETUP AND RESULTS

Test Facility

The Institute for Thermal Turbomachinery and Machine Dynamics at Graz University of Technology operates a 3MW compressor station in order to supply a couple of test facilities continuously with pressurized air. In the described subsonic test turbine facility, which is shown in Figure 2, the maximum pressure ratio is limited to 2 due to the inlet spiral casing. The maximum mass flow rate is 15 kg/s at a temperature at stage inlet of 100 °C.

A detailed description of the subsonic test turbine facility for aerodynamic, acoustic, and aeroelastic investigations (STTF-AAAI) is given in e.g. [6], [12].

Measurement Technique

A FRAPP was used to obtain the experimental data of the unsteady flow field. The cylindrical single-sensor probe was built and calibrated at Politecnico di Milano. The probe head diameter is 1.85mm and includes a miniaturized piezo-resistive sensor. With this probe it is possible to measure the unsteady total and static pressure. Operating the one-hole probe as a virtual three-sensor probe, also the yaw angle and the Mach number can be determined. This can be realized by turning the probe head into the flow direction and at least in two other rotational positions for each radial measurement point. During this measurements, the probe head was turned ± 45 deg relative to the flow direction.

The measurement time was 2s at each position with a sampling frequency of 500kHz. Measuring the three different rotational positions for each radial height at different times required a phase-resolve procedure using a phase-locked flow reconstruction. A trigger signal at each revolution was acquired to enable the determination of every start and end of a revolution.

Detailed descriptions of the measurement uncertainties of the used probe as well as for the variation of the operating parameters (pressure ratio, corrected speed, speed, total pressure and temperature at rig inlet) are given in [13].

Results

This section presents the results of the mode analysis applied on the unsteady data obtained from the FRAPP measurement downstream of the LPT stage depicted in Figure 2. The absolute values are normalised using the time averaged mean values of the corresponding flow field.

Figure 3 shows the development of the flow as contour plots of the normalised total pressure. These plots are aft looking forward views of a sector covering one TEGV pitch. As a consequence, stator pitches and 4.8 rotor pitches are included in the measured flow field.

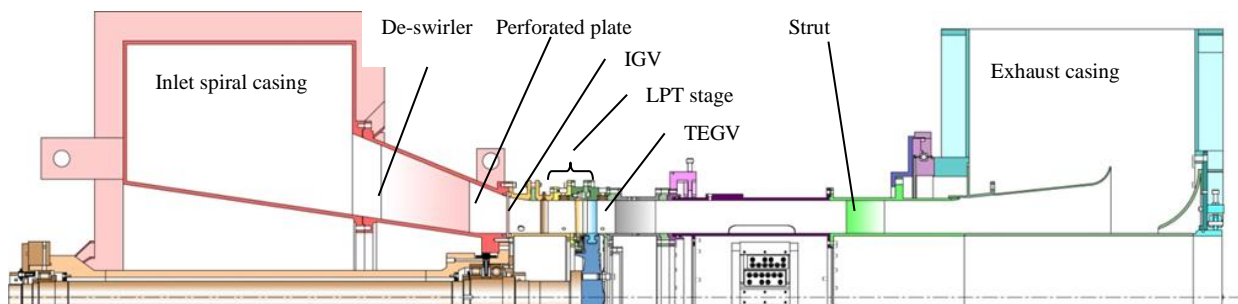


Figure 2: Meridional section of the STTF-AAAI

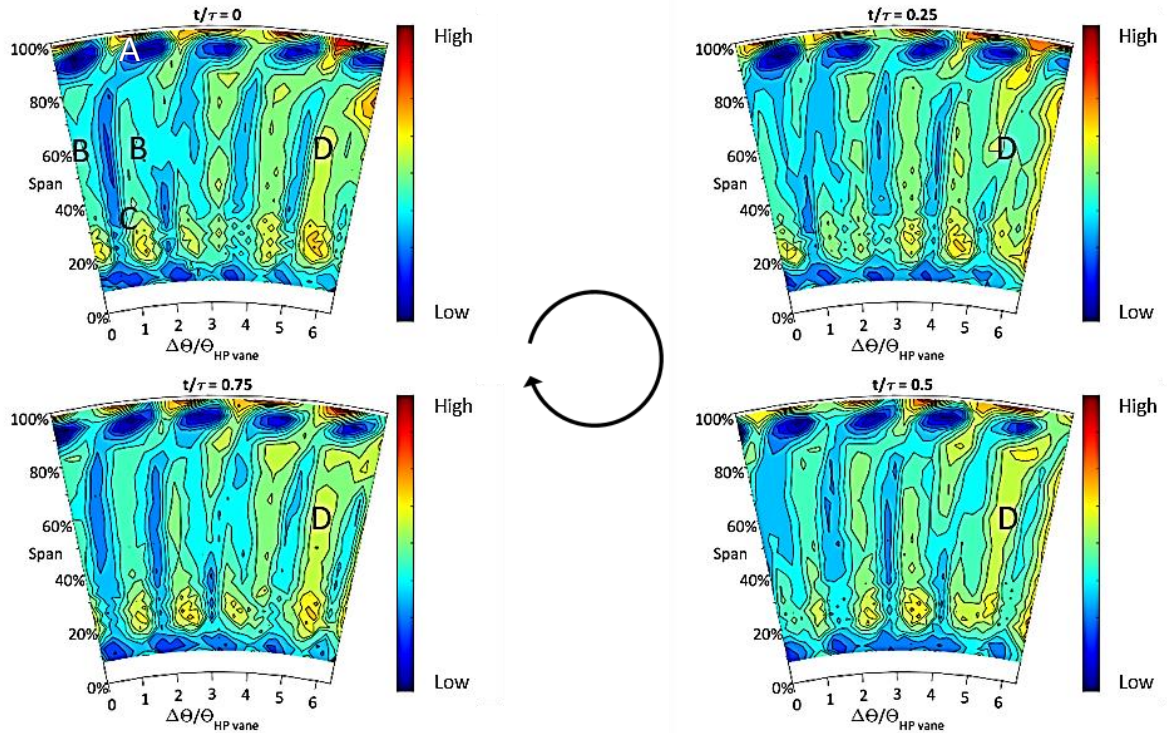


Figure 3: Time resolved distribution of the normalised total pressure downstream of the LPT rotor

The tip leakage vortex causes a low total pressure region, identified in the picture with the letter A. Just above, a very high total pressure area is recognizable. In [14] this high total pressure area was already identified as wall jet leakage flow. Smaller values of total pressure due to the rotor blade wakes are dominant in the region between 20% and 90% of the passage height. These areas are indicated in the picture with the letter B. Furthermore, the hub secondary vortex, which appears to be less intense than the tip leakage vortex, is marked in the figure with the letter C.

Moreover, it can be noticed that the measured total pressure field is not circumferentially uniform. In fact, lower values, marked with the letter D in the figure, can be observed in the right part of the plots.

This low total pressure pattern is not moving in time and therefore could be an indication of the potential effect due to the presence of a second stator row downstream of the LPT rotor.

The visualizations depicted in Figure 5 contain the modal structures related to the stator-rotor interactions for the first BPF. In particular, the figure shows the time-space diagrams of the total pressure and of the RMS value of the total pressure at two different radial positions, namely at 13% span (hub) and at 93% span (tip). The modes are represented with coloured dashed lines over two blade passing periods.

The rotor mode $m_{-B} = -72$ can be obtained from Equation (4) considering only the contribution of the rotor ($k = 0$). Since this mode

is only related to the rotor blades, it has a spinning velocity equal to the rotor rotational speed.

The trace due to the rotor mode is depicted in the time-space plots of Figure 5 as an inclined black dashed line which follows the mean trail of the rotor induced flow structures. While the inclined rotor trace is noticeable in both diagrams, it is in the plot representing the tip region (Figure 5 bottom) that its influence results highly dominant.

Table 1: Properties of the analysed modal structures

Mode	m	Ω	$\Delta\varphi_k/\Delta\varphi_{vane}$	Θ [deg]
m_{-B}	-72	$-\Omega$	-1.33	-53.1
m_{-B+V}	24	$3 \cdot \Omega$	4	76
m_{-B+2V}	120	$0.6 \cdot \Omega$	0.8	38.7
m_{-B-V}	-168	$-0.43 \cdot \Omega$	-0.57	-29.7

The main characteristics of this mode, evaluated from the equations presented in the sections above, are listed in Table 1 together with the ones of the other modes that will be introduced later on.

The azimuthal mode $m_{-B+V} = 24$, which is associated to the stator-rotor interaction, is depicted in the time-space plot with an orange dashed line. This pressure pattern rotates against the rotational direction of the rotor three times faster than the rotor. Comparing the plots referring to the hub (top)

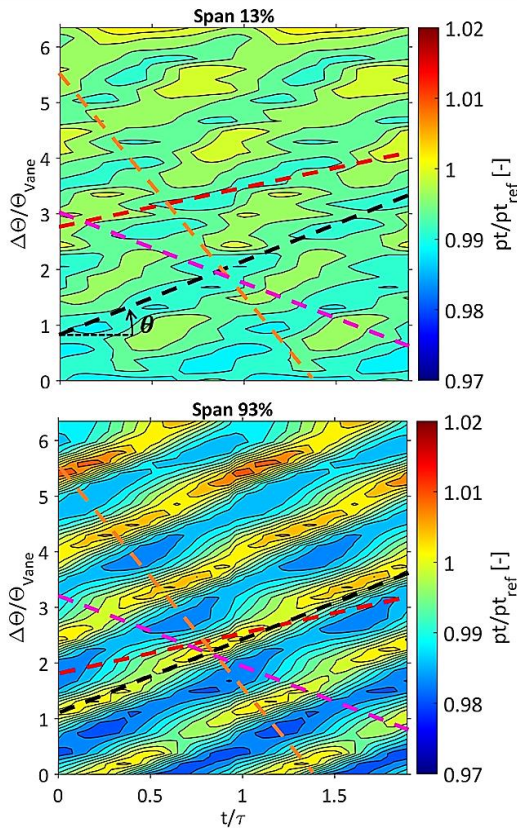


Figure 5: Time-space diagrams of the total pressure at 13% span (top) and at 93% span (bottom), with modes inclinations

and to the tip (bottom), this mode seems to have a higher relevance at the hub than at the tip, where the rotor mode $m_{-B} = -72$ is highly dominant.

Considering the index k is equal to 2, the mode order $m_{-B+2V} = 120$ is taken into consideration. Represented in Figure 5 as a magenta dashed line, this mode is generated by the stator-rotor interaction and rotates in the opposite direction of the rotor revolution.

The last relevant modal structure that will be analysed is the mode order $m_{-B-V} = -168$. This mode can be identified principally in the time-space plot of the tip, as a connection between the maxima of the total pressure, and is depicted as a dashed red line.

Results of the modal analysis

In order to obtain a more precise analysis of the modal structures which were identified in the time-space diagrams displayed above, the results of the modal decomposition previously described will be presented in this section.

In particular, Figure 4 shows the evaluated amplitude of the modal decomposition of the total pressure at the first BPF. The amplitudes of the rotor mode $m_{-B} = -72$ and of the interaction modes $m = 24, 120$ and -168 are plotted over the span height. This representation is applied to investigate the effects of the stator and rotor

induced flow structures and their interactions at different radial coordinates.

Observing Figure 4, it is possible to understand that the dominant modal structure over the whole span height is the rotor induced mode $m_{-B} = -72$. Additionally, the amplitude of this mode is substantially higher at the hub and at the tip than at mid-span, thus the fluctuations induced at the tip by the rotor tip leakage vortex and at the hub by the rotor hub passage vortex can be considered more intense than the fluctuations due to the wakes in the core flow.

It is interesting to highlight that the maximum value of the rotor mode amplitude is in the blade tip region. This results is in accordance with the time-space plot of the total pressure at 93% span (Figure 5 bottom), where the trace of the rotor was highly evident.

Regarding the stator-rotor interaction modes, mode $m_{-B+V} = 24$ is the most important one and its amplitude becomes comparable to the rotor induced unsteadiness in the hub region, especially at 12.5% span. Another modal structure that shows higher amplitudes at the hub is the mode $m_{-B+2V} = 120$. On the contrary, the amplitude of the interaction mode $m_{-B-V} = -168$ grows with the span height and reaches its maximum value at the blade tip.

In order to extend the analysis and the comparison between the different modes over the span height, the modal amplitudes corresponding to the time space-plots of Figure 5 are extracted from Figure 4 and are shown in Figure 6. First of all, it is possible to observe that, even though the rotor mode $m_{-B} = -72$ is the higher one both at the tip and at the hub, its amplitude is almost five times higher in the tip region. This fact confirms that the rotor driven structures are not only dominant in the flow field, but also have their stronger intensity in

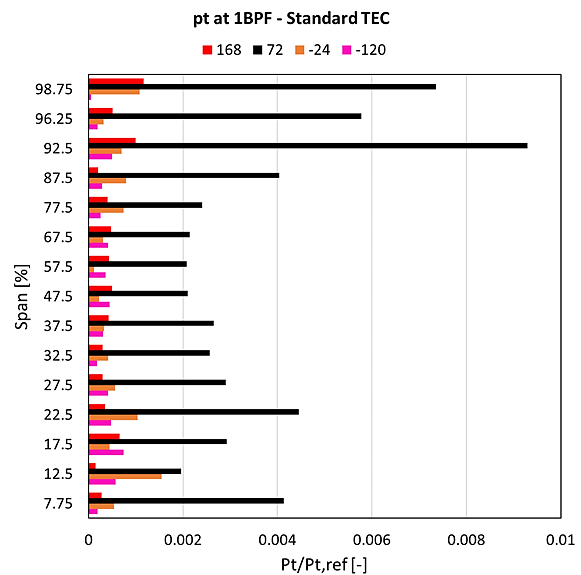


Figure 4: Normalised modal amplitudes of the total pressure over span height at the first BPF

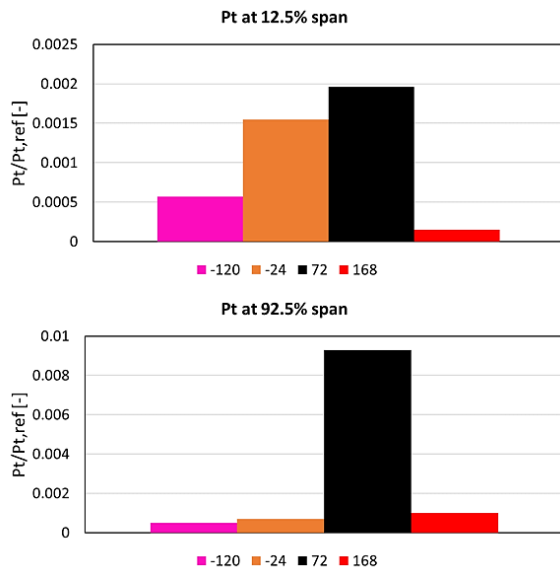


Figure 6: Detailed view of the normalized modal amplitudes of the total pressure at 13% span (top) and at 93% span (bottom)

the tip region.

With respect to the interaction modes, Figure 6 (top) shows that in the hub region the overall amplitudes of the modes $m = 24, 120$ is greater than the amplitude of the rotor mode alone. A first evidence of this behaviour of the modal amplitudes can be seen in the time-space plot representing the hub region in Figure 5. Thanks to the modal decomposition and the analysis over the span it is possible to quantify the effect of the stator-rotor interaction at the hub and to assess that they are more relevant in the lower section of the span.

CONCLUSION

This work reviews the theoretical background and the method behind the modal decomposition introduced by Tyler and Sofrin [1] and shows its ability to identify the effects of the aerodynamic unsteady interactions between stator and rotor rows.

The modal decomposition has been applied for the analysis of the unsteady measurements obtained in a 1.5 stage low pressure test turbine, operated under engine-relevant operating conditions, using a fast response aerodynamic pressure probe.

The flow unsteadiness is decomposed in circumferential lobed patterns for the first harmonic of the blade passing frequency.

The time-resolved results were used to recognise the features which characterise the unsteady flow field and time-space diagrams of the total pressure allowed to qualitatively decompose the unsteady flow field downstream of the rotor into its principal structures.

The evolution of the modal amplitudes in radial direction was studied in more details by means of azimuthal modal decomposition. It was

possible to recognise that the modal structure related to the rotor $m_{-B} = -72$ is dominant over the span height. Furthermore, the modal decomposition allowed to conclude that rotor tip leakage vortex represent the dominant source of the fluctuations induced by the rotor, as a consequence of the fact that the highest amplitude can be found in the tip region.

Additionally, the stator-rotor interaction modes were shown to have a higher importance in the hub region, where the amplitude of mode $m_{-B+V} = 24$ is comparable to the amplitude of the rotor related mode $m_{-B} = -72$.

In conclusion, the modal decomposition technique was described and successfully applied to study the main stator-rotor interaction mechanisms, and to classify the importance of the main modal patterns.

The results of this analysis can ultimately be employed in the context of aero-elastic and aero-acoustic analysis. Therefore, the evaluation of blade forces and noise emission in turbomachinery can be improved thanks to the evaluation of the modal structures of the unsteady aerodynamic flow fields.

ACKNOWLEDGEMENTS

The authors would like to thank Dr.techn. H.P. Pirker for operating the compressor station and his great support and discussions during all experimental investigations.

Further, the EU project VITAL (AIP4-CT-2004-012271) is acknowledged in which the TEC has been designed, manufactured and operated.

This work has been carried out in the framework of the national funded TAKE-OFF program within the research project EisenerZ (contract no. 855228) regarding the influence of inflow inhomogeneity on the vibration excitation of an LPT of a modern aircraft engine at Graz University of Technology at the Institute for Thermal Turbomachinery and Machine Dynamics. The authors therefore thank the Austrian Research Promotion Agency (FFG) and the Austrian Ministry for Transport Innovation and Technology (bmvit) for funding this project.

REFERENCES

- [1] Tyler, J. M.; Sofrin, T. G.; 1962. "Axial flow compressor noise studies", SAE Transaction, Vol. 70, pp.309-332
- [2] Lengani, D.; Selic, T.; Spataro, R.; Marn, A.; Göttlich, E.; 2012. "Analysis of the Unsteady Flow Field in Turbines by means of Modal Decomposition", Proceedings of ASME Turbo Expo, Paper-No. GT2012-68582

- [3] Zerobin, S.; Bauinger, S.; Marn, A.; Peters, A.; Heitmeir, F.; Göttlich, E.; 2017. "The Unsteady Flow Field of a Purged High Pressure Turbine Based on Mode Detection", Proceedings of ASME Turbo Expo, Paper-No. GT2017-63619
- [4] Lengani, D.; Paradiso, B.; Marn, A.; 2012. "A Method for the Determination of Turbulence Intensity by Means of a Fast Response Pressure Probe and its Application in a LP Turbine", Journal of Thermal Science, Vol. 21, No. 1
- [5] Camp, T. R.; Shin, H. W.; 1995. "Turbulence Intensity and Length Scale Measurements in Multistage Compressors", Journal of Turbomachinery, Vol. 117, pp. 38-46
- [6] Moser, M.; Tapken, U.; Enghardt, L.; Neuhaus, L.; 2009. "An Investigation of LP-Turbine blade/-vane interaction noise: Measurements in a 1.5 stage rig", IMechE Journal of Power and Energy, Vol. 223, No. 6, pp. 687-695
- [8] Selic, T.; Marn, A.; Schönleitner, F.; Hoeger, M.; Broszat, D.; Heitmeir, F.; 2015. "Comparison of an Acoustically Optimized and an Aerodynamically Optimized Exit Guide Vane", Proceedings of 11th ETC
- [9] Marn, A.; Selic, T.; Schönleitner, F.; Zerobin, S.; 2015. "Acoustic Comparison of Different Turbine Exit Guide Vane Designs Part 2: Experimental Analysis", 21st AIAA/CEAS Aeroacoustics Conference
- [10] Morfey, C.; 1971. "Sound Transmission and Generation in Ducts with Flow", Journal of Sound and Vibration, Vol. 14, No. 1, pp. 37-55
- [11] Lengani, D.; Santner, C.; Spataro, R.; Göttlich, E.; 2012. "Analysis tools for the unsteady interactions in a counter-rotating two-spool turbine rig", Experimental Thermal Fluid Science, Vol. 42, pp. 248-257
- [12] Simonassi, L.; Zenz, M.; Zerobin, S.; Heitmeir, F.; Marn, A.; 2018. "On the Influence of an Acoustically Optimized Turbine Exit Casing onto the Unsteady Flow Field Downstream of a Low Pressure Turbine Rotor", Proceedings of ASME Turbo Expo, Paper-No. GT2018-76725
- [13] Persico, G.; Gaetani, P. and Guardone, A.; 2005. "Design and analysis of new concept fast-response pressure probes", Measurement Science and Technology, 16, pp. 1741-1750
- [14] Lengani, D.; Paradiso, B.; Marn, A.; Göttlich, E.; 2012. "Identification of Spinning Mode in the Unsteady Flow Field of a Low Pressure Turbine", Journal of Turbomachinery, Vol. 134